Evaluation of Lung Involvement in COVID-19 Pneumonia Based on Ultrasound Images

Zhaoyu Hu
fudan university https://orcid.org/0000-0003-3490-1467
Zhenhua Liu
Shanghai Jiao Tong University Medical School Affiliated Ruijin Hospital
Yijie Dong
Shanghai Jiao Tong University Medical School Affiliated Ruijin Hospital
Jianjian Liu
Shanghai Public Health Clinical Center
Bin Huang
Hangzhou Children's Hospital
Aihua Liu
the sixth hospital of wuhan
Jingjing Huang
Shanghai Public Health Clinical Center
Xujuan Pu
Shanghai Public Health Clinical Center
Xia Shi
Shanghai Public Health Clinical Center
Jinhua Yu
Fudan University
Yang Xiao (yang.xiao@siat.ac.cn)
Institute of Biomedical and Health Engineering Shenzhen Institutes of Advanced Technology
Hui Zhang
Zhongshan Hospital Fudan University
Jianqiao Zhou
Shanghai Jiao Tong University Medical School Affiliated Ruijin Hospital

Research

Keywords: ultrasound, lung involvement, classification, COVID-19, neural network

Posted Date: September 4th, 2020

DOI: https://doi.org/10.21203/rs.3.rs-70092/v1

Version of Record: A version of this preprint was published at BioMedical Engineering OnLine on March 20th, 2021. See the published version at https://doi.org/10.1186/s12938-021-00863-x.

Abstract

Background: Lung ultrasound (LUS) can be an important imaging tool for the diagnosis and assessment of lung involvement. In this study, we determined the ultrasound manifestations of the lung associated with COVID-19 pneumonia, and obtained the ultrasound image changes of the patients from the initial diagnosis to rehabilitation.

Methods: The purpose of this study is to establish a lung involvement assessment model based on deep learning. A channel attention classification method based on squeeze-and-excitation network combining with ResNeXt (SE_ResNeXt) is proposed, which can automatically learn the importance of different channel features, so as to achieve selective learning of channels and further achieve more accurate classification results.

Results and conclusion: Among 104 patients' data from multicenter and multi-mode ultrasound, the diagnostic model can achieve 97.11% accuracy. The lung involvement severity of COVID-19 pneumonia and the trend of lesion were evaluated quantitatively.

1. Introduction

BY August 31, 2020, 25,350,668 confirmed cases and 846,818 deaths of novel coronavirus 2019 (COVID-19) disease in the world have been reported. COVID-19 disease is reported in 212 countries [1]. The World Health Organization has announced that the COVID-19 disease has become a global pandemic [2]. Rapid diagnosis and assessment of the severity of the disease are highly required with the increasing number of cases.

The current gold standard for the diagnosis of COVID-19 disease is the reverse transcription polymerase chain reaction (RT-PCR) analysis of respiratory specimens [3]. However, due to incorrect sampling of nasopharyngeal swabs, the false negative rate is high [4]. Delayed diagnosis will cause the spread of the disease and the aggravation of the patient's condition. Computed tomography (CT) is the main method for diagnosing and evaluating the severity of patients with COVID-19 pneumonia [5, 6]. However, CT also has the following problems in lung diagnosis. First, CT diagnosis is costly and has radiation [7]. In unstable critical patients, CT examination is not easy to perform. In addition, patients who are sensitive to radiation, such as pregnant women, need to avoid the radiation caused by CT examination. Second, it is of great clinically significance to determine whether there is pulmonary airway obstruction in patients with COVID-19 pneumonia. CT can only obtain static images and cannot evaluate the movement of gas in the bronchi and bronchiole in real time.

As a non-radiation medical imaging method, ultrasound is highly sensitive to the diagnosis of various lung diseases [8]. Studies have shown that lung ultrasonography (LUS) can be an important imaging tool for the diagnosis of pneumonia and the assessment of the degree of lung involvement [9]. For example, Liu et al. proved the value of bedside LUS in the diagnosis of community-acquired pneumonia. With CT as the gold standard, the diagnosis of community-acquired pneumonia by LUS has reached 96.1% of

accuracy, and the diagnostic efficiency far exceeds chest X-ray [10]. Bouhemad et al. [11] and Silvia et al. [12] reported that LUS has potential to be a key tool for early ventilator-associated pneumonia (VAP) diagnosis. Within the technical period required for Broncho alveolar lavage analysis, LUS is an ideal decision-making tool for antimicrobial management. LUS was used as a good imaging method for diagnosing pneumonia in many institutions. The advantages of LUS are that it is inexpensive, non-radiating and easy to obtain, and can be checked at bedside, especially for patients with severe pneumonia [13, 14].

In this study, we propose a channel attention classification method based on Squeeze-and-Excitation network combining with ResNeXt (SE_ResNeXt), which can automatically learn the importance of different channel features. In order to make better use of this feature, the traditional methods of gradient field and K-Means clustering are used to extract feature maps from original ultrasound image as additional channel information. In addition, we determined the ultrasound manifestations of the lung associated with COVID-19 pneumonia, and obtained the ultrasound image changes of the patients from the initial diagnosis to rehabilitation.

2. Results

2.1. SE_ResNeXt Classification Accuracy

Table 1 summarizes the results of classification accuracy compared to other methods. K and G represent K-Means clustering and gradient field respectively in the table. It can be seen that the proposed SE_ResNeXt_K+G outperforms the original SE_ResNeXt, which has 98.56%, 98.21%, 97.11% and 91.79% average accuracy on Stork, Mindray, Stork & Mindray and Stork & Mindray & Philips, respectively. Significant improvements on three datasets have been achieved by using gradient field and K-Means clustering, the accuracy is further enhanced.

Table 1. Comparison of classification accuracy on different dataset.

Method	S[1] (%)	M[2] (%)	S&M (%)	S&M&P[3] (%)
ResNet	96.66	95.76	95.55	89.73
SE_Inception	95.94	96.03	95.13	87.92
SE_Inception_ResNet	96.84	96.21	95.40	88.21
SE_ResNeXt	96.73	96.39	96.03	90.84
SE_ResNeXt_K[4]	98.43	98.21	97.02	91.67
SE_ResNeXt_K+G[5]	98.56	98.21	97.11	91.79

[1]S = Stork dataset accuracy, [2]M = Mindray dataset accuracy, [3]P = Philips dataset accuracy; [4]K = K-Means

clustering, ^{5}G = gradient field.

The normalized confusion matrixes of classification on three datasets by our proposed method are provided in Fig. 1. For Stork dataset, except for a small part of the classification of B1-line into B1 & B2-line, the remaining classification accuracy rate is close to 100%; for Stork & Mindray dataset, a small percentage of B2-line is classified as B1-line, and B1-line is classified as A & B-line; for Stork & Mindray & Philips dataset, a large part of B2-line and B1-line is mistakenly classified into B1 & B2-line. In short, the classification accuracy of A-line and consolidation on three datasets can reach nearly 100%. Misclassification generally occurs in the fusion classification of two categories.

2.2. Distribution of datasets

Fig. 2 depicts the distribution of expert manual labels classification of 5704 ultrasound images in three datasets. Because most of the patients with COVID-19 are patients with severe lung involvement, the data of A-line and A&B-line is few. In the actual experiment, we use combining datasets and data augmentation to solve the problem of sample imbalance.

2.3. Evaluation on the trend of the degree of lung involvement

After obtaining the trained SE_ResNeXt, we independently test the videos of 8 patients' (1 frame per second), which have been examined multiple times (3 times or more), and perform the classified class according to the method in section 2.4. PCO2 is a great indicator of respiratory function and closely related factor of acid–base homeostasis, reflecting the amount of acid in the blood. The correlation between the score obtained and CO2 partial pressure (PCO2) was analyzed by Pearson correlation analysis, and the correlation is shown in Fig. 3. The Pearson correlation coefficient is 0.71 ($P < .001$). In the graph, the darker the color shows, the higher the frequency of occurrence is. The graph shows that the score of SE_ResNeXt is in the range of 2.7-3.4, which has a higher correlation with PCO2.

In addition, two patients with multiple examinations of SE_ResNeXt score and PCO2 are shown in Fig. 4. We follow the three lines of parasternal line (PSL), anterior axillary line (AAL) and posterior axillary line (PAL) in [15] to divide the left and right sides of lungs into four areas (L1-L4 and R1-R4). Only one picture is shown in the figure, but in the actual scoring, we average the scores of multiple pictures after framing the video of a certain partition to obtain the specific score in the figure.

In short, our classification and scoring system not only reflects the degree of lung involvement of patient, but also helps doctors combine this score with other indicators to evaluate the patient's lung disease and even the entire person's condition. It is more beneficial to use this scoring system to improve the nursing level of patients with pneumonia, and enhance their support to the clinical decision-making process for the pneumonia-management cascade.

3. Discussion

J. Rouby et al. assessed lung involvement by scoring eight areas' sonograms [16], while the sonograms need to be manually identified by doctors, which is time-consuming and labor-intensive. Nowadays, there have been some research on the automatic classification of sonograms, but most of them are only for detecting B-line of sonograms [17, 18].

In this paper, we proposed a classification network for fully automatic assessment of lung involvement in COVID-19 patients. The lung ultrasound images of these patients are classified into six types of sonograms, the classification results were quantitatively scored to obtain the total scores of 8 regions, and the correlation analysis between the scores and the PCO2, which is the most relevant to lung involvement, was obtained. As a result, a Pearson correlation coefficient of 0.71 was obtained, indicating that our classification scores can reflect the lung involvement of COVID-19 patients. It is useful to choose the correct treatment method according to the serious situation.

We try to train with data from one center, and the data from another center was used for independent testing. But Stork dataset has only 58 consolidation images, if we use trained Stork model to predict Mindray's consolidation data (1136 images), the accuracy of independent testing will be greatly reduced in this category of classification and vice versa.

In the final result, the increase of adding the gradient field is very small, which is related to our dataset, because normal people will have a large number of A-lines, and most of the data we collected are patients. If there are a large number of A-line in the data, the advantage of adding gradient field will be revealed. Our network is more robust to multi-center and multi-machine data, because the gradient field and K-Means information extracted by traditional methods are highly robust, useful information can also be extracted under the condition that the imaging parameters of the original image have a large discrepancy.

4. Conclusion

In this paper, for the ultrasound images of the lungs of patients with COVID-19 pneumonia, we propose a classification network that combines traditional methods with channel attention, and score the predicted categories. The final score reflects the degree of lung involvement in the patient and helps doctors to combine other indicators to assess the overall condition and disease trend of COVID-19 patients.

5. Materials And Methods

5.1. Ultrasound Data Acquisitions

In ultrasound imaging, the degree of lung involvement is related to several typical sonograms. A-line is a horizontal reverberation artifact of pleura caused by multiple reflections, representing the normal lung surface [19]. B-line represents the interlobular septum, which is denoted by a discrete laser like vertical hyperechoic artifact that spreads to the end of the screen, and it can be represented as B1-line [20]. Fusion B-line is a sign of pulmonary interstitial syndrome, which shows a large area filled with B-line in

intercostal space, and it can be represented as B2-line [15]. Pulmonary consolidation is characterized by a liver like echo structure of the lung parenchyma, with a thickness of at least 15 mm [16] as shown in Fig. 5.

We use three datasets from four medical centers to build and evaluate the model: Ultrasound images collected by Stork ultrasound system (Stork Healthcare Co., Ltd. Chengdu, China) at Ruijin Hospital, Mindray ultrasound system (Mindray Medical International Limited, Shenzhen, China) at Shanghai Public Health Center, Philips ultrasound system (Philips Medical Systems, Best, the Netherlands) at Wuhan Sixth People's Hospital and Hangzhou Infectious Disease Hospital. Stork dataset was collected with H35C (2-5MHz) convex array transducer, Mindray dataset with SC5-1 (1-5 MHz) convex array transducer, and Philips dataset with Epiq 5, Epiq 7 C5-1 (1-5MHz) convex array transducer.

5.2. Feature map extraction by traditional methods

As shown in Fig. 5, different ultrasound sonograms represent different degrees of lung involvement. The data for this study comes from multiple centers and multiple devices. In order to make the diagnostic model more robust, we used traditional image processing methods to extract features that are not sensitive to imaging parameters, and then put the extracted feature map together with the original ultrasound image into the deep learning model. Since gradient field is highly sensitive to parallel echo rays of A-line, and K-Means clustering is highly sensitive to the laser beam-like echo bars of B-line as shown in Fig. 6, we extracted the gradient field and K -Means clustering images as two feature maps.

5.3. SE_ResNeXt classification model

Overview of the proposed SE_ResNeXt for lung congestion degree classification is provided in Fig. 7. Take one input as an example, after obtaining the gradient field and K-Means clustering information, we combine these two types of information as additional channel information with the original image as a three-channel input (W × H × 3). Then perform a squeeze operation on the input image, that is, global average pooling to encode the entire spatial feature on a channel as a global feature.

$$F_{sq}(U) = \frac{1}{W \times H} \sum_{i=1}^{W} \sum_{j=1}^{H} U(i,j),\ U \in R^{W \times H \times 3} \qquad (1)$$

The squeeze operation gets the global description feature; another operation is required to capture the relationship between the channels, namely the excitation operation.

$$F_{ex}(F_{sq}(U)) = \sigma(W_2 \mathrm{Re}LU(W_1 F_{sq}(U))) \qquad (2)$$

Among them, $W_1 \in R^{\frac{3}{r} \times 3}$, $W_2 \in R^{3 \times \frac{3}{r}}$, dimension reduction coefficient is a hyperparameter. The excitation operation can learn the nonlinear relationship between channels. Finally, the learned activation value of

each channel (sigmoid activation) is multiplied by the original feature on:

$$y = F(U, F_{ex}(F_{sq}(U))) = U \cdot F_{ex}(F_{sq}(U)), U \in R^{W \times H \times 3} \quad (3)$$

The entire network has learned the weight coefficients of each channel, which makes the model more discriminative to the characteristics of each channel. A-line can learn more from gradient field channels, and B-line can learn more from K-Means clustering channels, which can reach the channel attention effect.

In order to fully take the advantages of channel attention, we choose ResNeXt as the backbone network for classification. ResNeXt [21] is a combination of ResNet [22] and Inception [23], which improves accuracy through wider or deeper networks. Each of its blocks is a measurable dimension in addition to the width and depth dimensions. It inherits the strategy of repeating layers of ResNet, but increases the number of paths, and uses split conversion and merge strategies in a simple and scalable manner. So in this classification task we adopt Inception's split-transform-merge idea to widen the network, which basically does not change the complexity of the model while increasing the accuracy. In addition, the topology of the network is the same for every aggregated topology that also reduces the design burden. The specific network block is provided in Fig. 8.

Detailed procedure are as follows: (1) Extract most common 6 types of datasets in Fig. 5 from the training set in equal proportions randomly to prevent sample imbalance and ensure that each category can be learned. (2) Enhance the data by rotation and normalize the intensity of the image. (3) Select the classifier with the best performance and test it on the test set to obtain the corresponding prediction results.

5.4. Establishment of scoring standards

We predicted the patient's per part ultrasound video of multiple examinations through the trained SE_ResNeXt, and classify and score sonograms according to [24]. A-line indicates that the patient is normally ventilated, with a score of 0; A & B-line indicates that the patient has mild lung ventilation loss, with a score of 1; B1-line indicates that the patient has moderate lung ventilation loss, with a score of 2; B1 & B2-line indicates that the patient has severe lung loss of ventilation, with a score of 2.5; B2-line indicates that the patient has very severe loss of lung ventilation, with a score of 3; Consolidation indicates that the patient has a solid lung change characterized by dynamic air bronchial signs, with a score of 4. After the classification result is quantified, the sum is divided by all the frames to obtain the final lung function severity score, which is 0 to 4.

5.5. Training Strategy

For the Stork, Mindray, Stork & Mindray and Stork & Mindray & Philips dataset, we use 3-fold cross-validation to verify the performance of the classifier. All the images are resized to 32 × 32, and a training batch consist of 128 randomly selected images. We regularize the model by using dropout during

training, and the neural network parameters are then learned by maximizing log-likelihood using the Momentum optimizer with an initial learning rate of 0.1, then every 30 epochs, the learning rate dropped by 10 times, stochastically minimizing the cross-entropy between annotated labels and predictions.

Abbreviations

LUS: Lung ultrasound; COVID-19: novel coronavirus 2019; RT-PCR: reverse transcription polymerase chain reaction; CT: Computed tomography; VAP: ventilator-associated pneumonia; PCO2: CO2 partial pressure; PSL: parasternal line; POI: points of interest; AAL: anterior axillary line; PAL: posterior axillary line.

Declarations

Acknowledgements

The authors are grateful to all study participants.

Funding

This research was funded by the National Natural Science Foundation of China, grant number 91959127 and by the Shanghai Science and Technology Action Innovation Plan, grant number 19441903100.

Author's contributions

ZH and JhY suggested the algorithm for image analysis, ZH implemented it and analysed the experimental results; ZL, HZ, JL, BH, AL, XS and YX collected experimental data and provided clinical guidance; AL, JH, XP and YD consulted the obtained result. All authors read and approved the final manuscript.

Availability of data and materials

Not applicable

Ethics approval and consent to participate

Bioetic Commission for this study is not necessary

Consent for publication

Not applicable

Competing interests

The authors declare that they have no competing interests

Author details

[1] Department of Electronic Engineering, Fudan University, Shanghai 200433, China.

[2] Department of Ultrasound, Ruijin Hospital, Shanghai Jiaotong University School of Medicine, Shanghai 200025, China.

[3] Department of Ultrasound, Shanghai Public Health Clinical Center, Shanghai 201508, China.

[4] Department of Ultrasound, Xixi Hospital of Hangzhou, Hangzhou 310023, China.

[5] Department of Ultrasound, The Six Hospital of Wuhan, Affiliated Hospital of Jianghang University, Wuhan, China.

[6] Institute of Biomedical and Health Engineering Shenzhen Institutes of Advanced Technology, Chinese Academy of Sciences.

References

1. Coronavirus resource center JHUoM. COVID-19 Case Tracker: Follow global cases and trends. Updated daily. https://coronavirus.jhu.edu. Published 2020.
2. Coronavirus disease (COVID-19) Pandemic WHO. https://www.who.int/emergencies/diseases/novel-coronavirus-2019. Published 2020.
3. China CJVsTecoaoo. Novel Coronavirus Pneumonia Emergency Response Epidemiology Team. 2019.
4. Hao W, Li M. Clinical diagnostic value of CT imaging in COVID-19 with multiple negative RT-PCR testing. Travel Med Infect Dis 2020:101627. doi: 10.1016/j.tmaid.2020.101627
5. Bernheim A, Mei X, Huang M, Yang Y, Fayad ZA, Zhang N, Diao K, Lin B, Zhu X, Li K, Li S, Shan H, Jacobi A, Chung M. Chest CT Findings in Coronavirus Disease-19 (COVID-19): Relationship to Duration of Infection. Radiology 2020:200463. doi: 10.1148/radiol.2020200463
6. Pan F, Ye T, Sun P, Gui S, Liang B, Li L, Zheng D, Wang J, Hesketh RL, Yang L, Zheng C. Time Course of Lung Changes On Chest CT During Recovery From 2019 Novel Coronavirus (COVID-19) Pneumonia. Radiology 2020:200370. doi: 10.1148/radiol.2020200370
7. Self WH, Courtney DM, McNaughton CD, Wunderink RG, Kline JA. High discordance of chest x-ray and computed tomography for detection of pulmonary opacities in ED patients: implications for diagnosing pneumonia. Am J Emerg Med 2013;31(2):401-405. doi: 10.1016/j.ajem.2012.08.041
8. Parra A, Perez P, Serra J, Roca O, Masclans JR, Rello J. Pneumonia and Lung Ultrasound in the Intensive Care Unit. Chest 2014;145(3). doi: 10.1378/chest.1806646
9. Aghdashi M, Broofeh B, Mohammadi A. Diagnostic performances of high resolution trans-thoracic lung ultrasonography in pulmonary alveoli-interstitial involvement of rheumatoid lung disease. Int J Clin Exp Med 2013;6(7):562-566.

10. Liu XL, Lian R, Tao YK, Gu CD, Zhang GQ. Lung ultrasonography: an effective way to diagnose community-acquired pneumonia. Emerg Med J 2015;32(6):433-438. doi: 10.1136/emermed-2013-203039
11. Bouhemad B, Dransart-Raye O, Mojoli F, Mongodi S. Lung ultrasound for diagnosis and monitoring of ventilator-associated pneumonia. Ann Transl Med 2018;6(21):418. doi: 10.21037/atm.2018.10.46
12. Mongodi S, Via G, Girard M, Rouquette I, Misset B, Braschi A, Mojoli F, Bouhemad B. Lung Ultrasound for Early Diagnosis of Ventilator-Associated Pneumonia. Chest 2016;149(4):969-980. doi: 10.1016/j.chest.2015.12.012
13. Berlet T, Etter R, Fehr T, Berger D, Sendi P, Merz TM. Sonographic patterns of lung consolidation in mechanically ventilated patients with and without ventilator-associated pneumonia: a prospective cohort study. J Crit Care 2015;30(2):327-333. doi: 10.1016/j.jcrc.2014.11.021
14. Xia Y, Ying Y, Wang S, Li W, Shen H. Effectiveness of lung ultrasonography for diagnosis of pneumonia in adults: a systematic review and meta-analysis. J Thorac Dis 2016;8(10):2822-2831. doi: 10.21037/jtd.2016.09.38
15. Volpicelli G, Elbarbary M, Blaivas M, Lichtenstein DA, Mathis G, Kirkpatrick AW, Melniker L, Gargani L, Noble VE, Via G, Dean A, Tsung JW, Soldati G, Copetti R, Bouhemad B, Reissig A, Agricola E, Rouby JJ, Arbelot C, Liteplo A, Sargsyan A, Silva F, Hoppmann R, Breitkreutz R, Seibel A, Neri L, Storti E, Petrovic T, Icc-Lus I-L. International evidence-based recommendations for point-of-care lung ultrasound. Intens Care Med 2012;38(4):577-591. doi: 10.1007/s00134-012-2513-4
16. Rouby JJ, Arbelot C, Gao Y, Zhang M, Lv J, An Y, Wang C, Bin D, Barbas CSV, Dexheimer Neto FL, Prior Caltabeloti F, Lima E, Cebey A, Perbet S, Constantin JM, group As. Training for Lung Ultrasound Score Measurement in Critically Ill Patients. Am J Respir Crit Care Med 2018. doi: 10.1164/rccm.201802-0227LE
17. Brusasco C, Santori G, Bruzzo E, Tro R, Robba C, Tavazzi G, Guarracino F, Forfori F, Boccacci P, Corradi F. Quantitative lung ultrasonography: a putative new algorithm for automatic detection and quantification of B-lines. Crit Care 2019;23(1):288. doi: 10.1186/s13054-019-2569-4
18. van Sloun RJG, Demi L. Localizing B-Lines in Lung Ultrasonography by Weakly Supervised Deep Learning, In-Vivo Results. IEEE J Biomed Health Inform 2020;24(4):957-964. doi: 10.1109/JBHI.2019.2936151
19. Liu J, Copetti R, Sorantin E, Lovrenski J, Rodriguez-Fanjul J, Kurepa D, Feng X, Cattaross L, Zhang H, Hwang M, Yeh TF, Lipener Y, Lodha A, Wang JQ, Cao HY, Hu CB, Lyu GR, Qiu XR, Jia LQ, Wang XM, Ren XL, Guo JY, Gao YQ, Li JJ, Liu Y, Fu W, Wang Y, Lu ZL, Wang HW, Shang LL. Protocol and Guidelines for Point-of-Care Lung Ultrasound in Diagnosing Neonatal Pulmonary Diseases Based on International Expert Consensus. J Vis Exp 2019(145). doi: 10.3791/58990
20. Francisco MJN, Rahal AJ, Vieira FA, Silva PS, Funari MB. Advances in lung ultrasound. Einstein (Sao Paulo) 2016;14(3):443-448. doi: 10.1590/S1679-45082016MD3557
21. Xie SN, Girshick R, Dollar P, Tu ZW, He KM. Aggregated Residual Transformations for Deep Neural Networks. Proc Cvpr Ieee 2017:5987-5995. doi: 10.1109/Cvpr.2017.634

22. He KM, Zhang XY, Ren SQ, Sun J. Deep Residual Learning for Image Recognition. 2016 Ieee Conference on Computer Vision and Pattern Recognition (Cvpr) 2016:770-778. doi: 10.1109/Cvpr.2016.90
23. Szegedy C, Liu W, Jia YQ, Sermanet P, Reed S, Anguelov D, Erhan D, Vanhoucke V, Rabinovich A. Going Deeper with Convolutions. 2015 Ieee Conference on Computer Vision and Pattern Recognition (Cvpr) 2015:1-9. doi: DOI 10.1109/cvpr.2015.7298594
24. Ranzani OT, Taniguchi LU, Torres A. Severity scoring systems for pneumonia: current understanding and next steps. Curr Opin Pulm Med 2018;24(3):227-236. doi: 10.1097/Mcp.0000000000000468

Figures

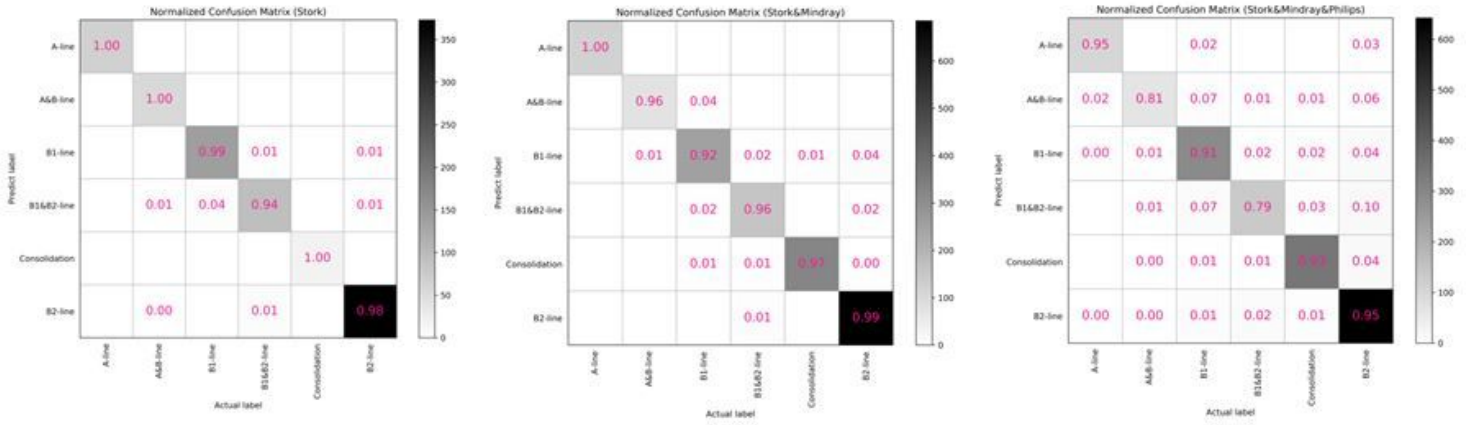

Figure 1

The normalized confusion matrix of classification on three datasets by our proposed method.

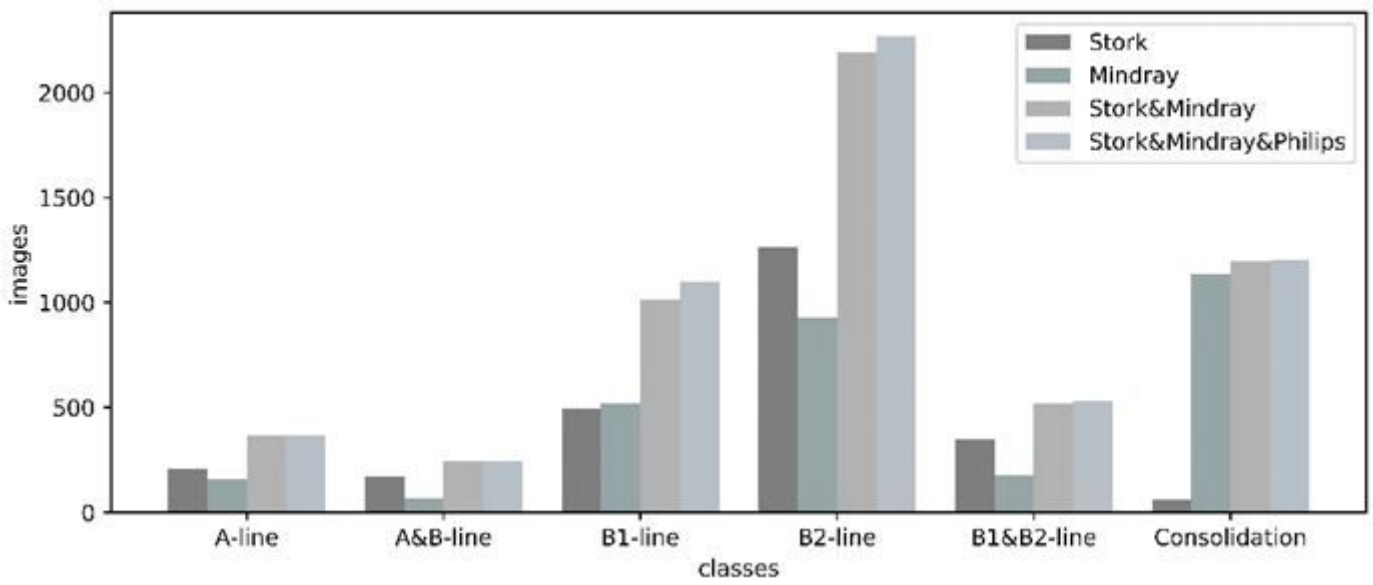

Figure 2

Distribution of expert manual labels of 5704 ultrasound images in three datasets.

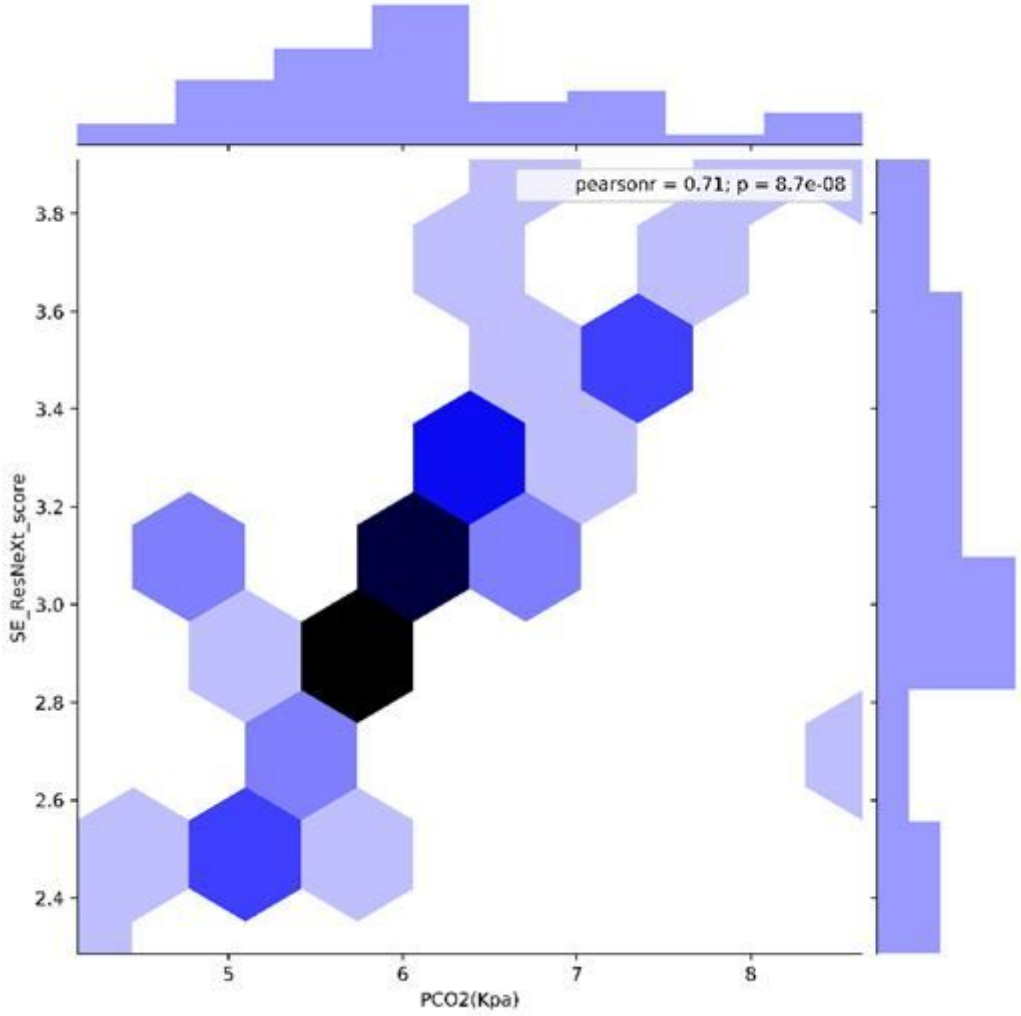

Figure 3

Scatter plot between classification score of SE_ResNeXt and CO2 partial pressure (PCO2).

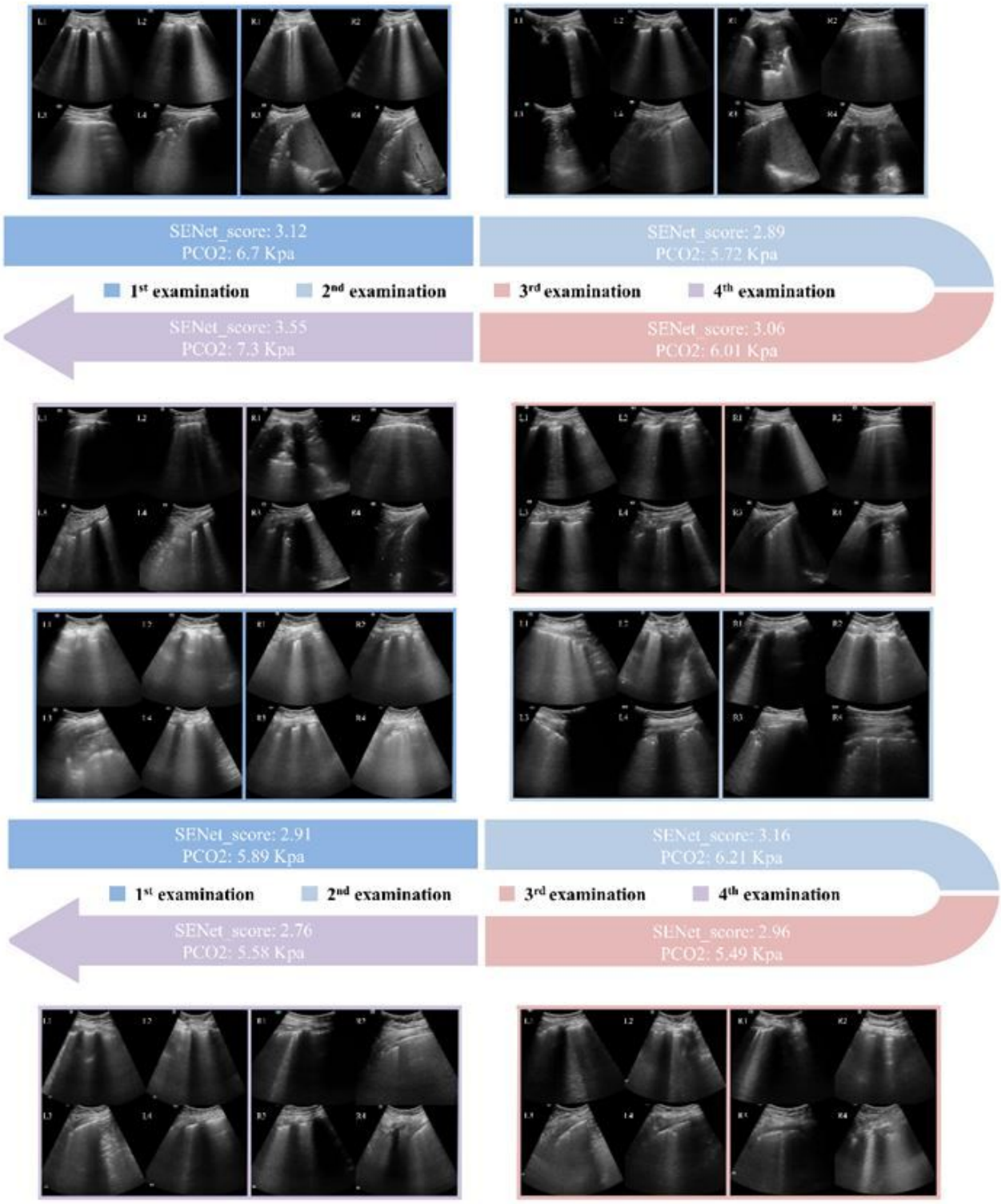

Figure 4

Two patients with multiple examinations of SE_ResNeXt score and PCO2.

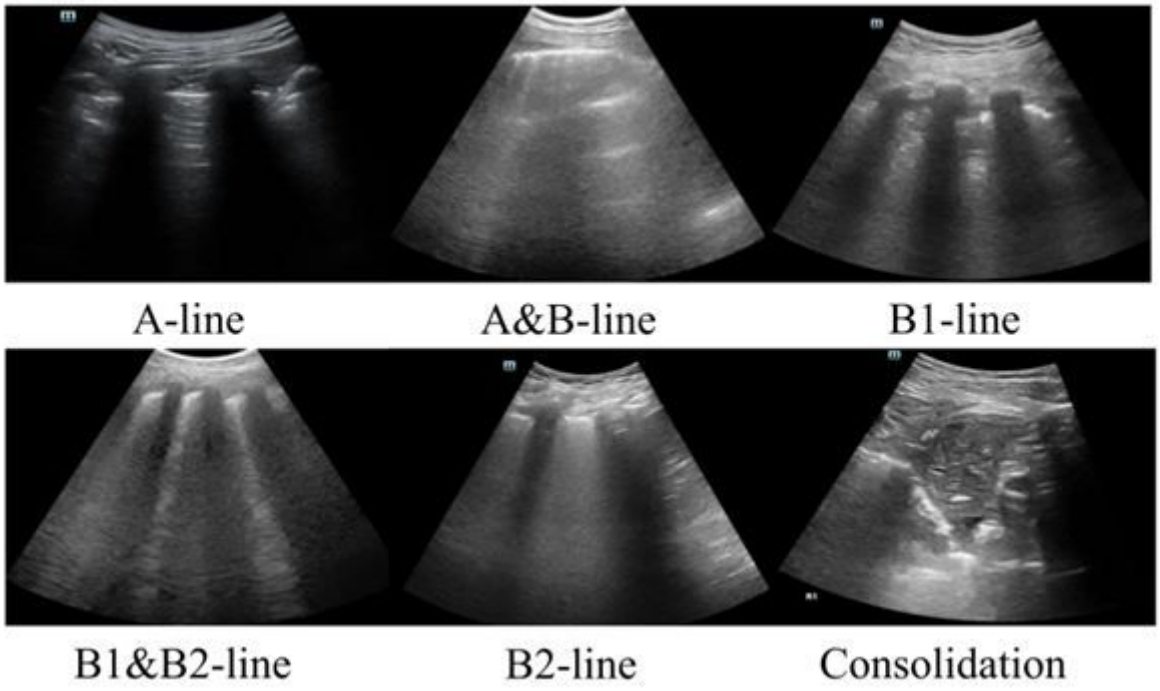

Figure 5

Different ultrasound sonograms in lung examination.

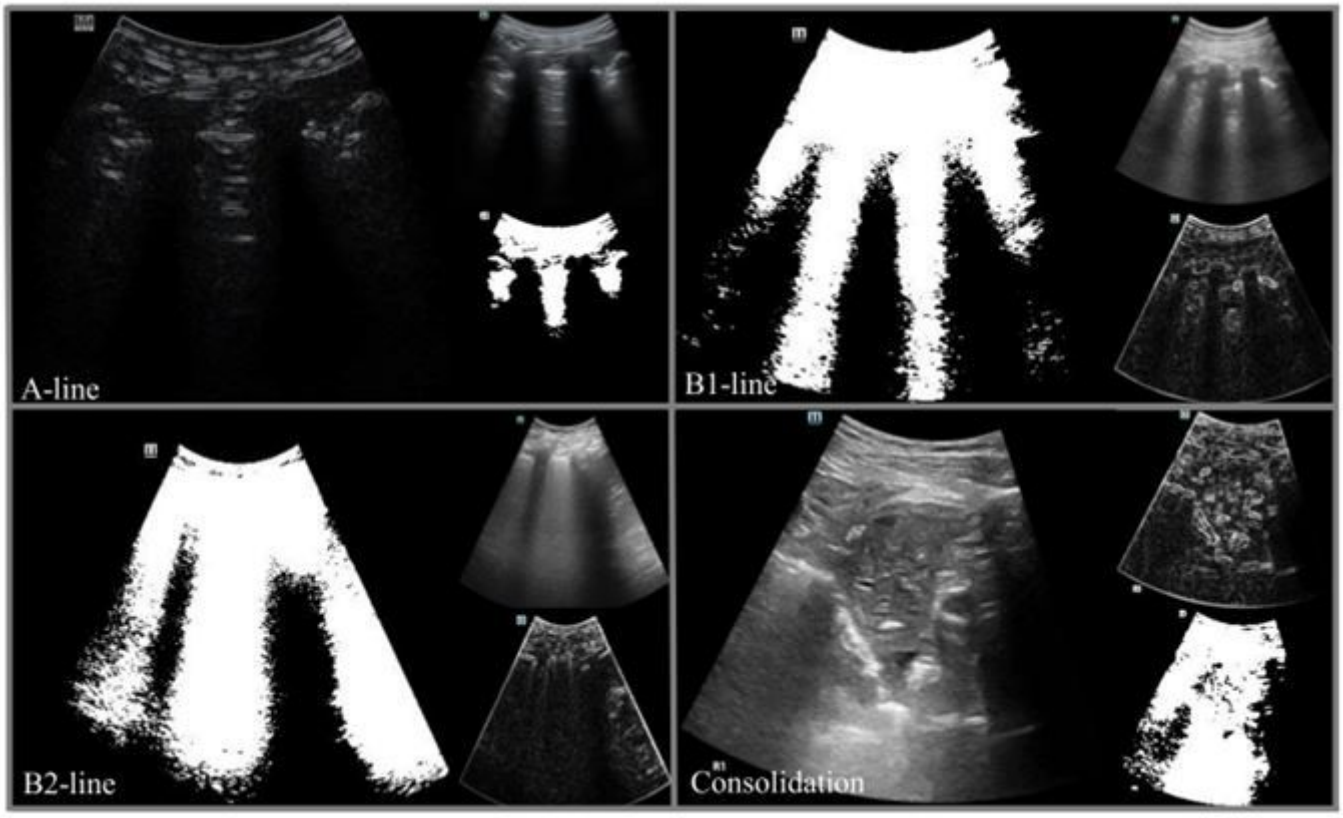

Figure 6

Traditional method information extraction results. The largest picture represents the most sensitive channel among the four sonograms.

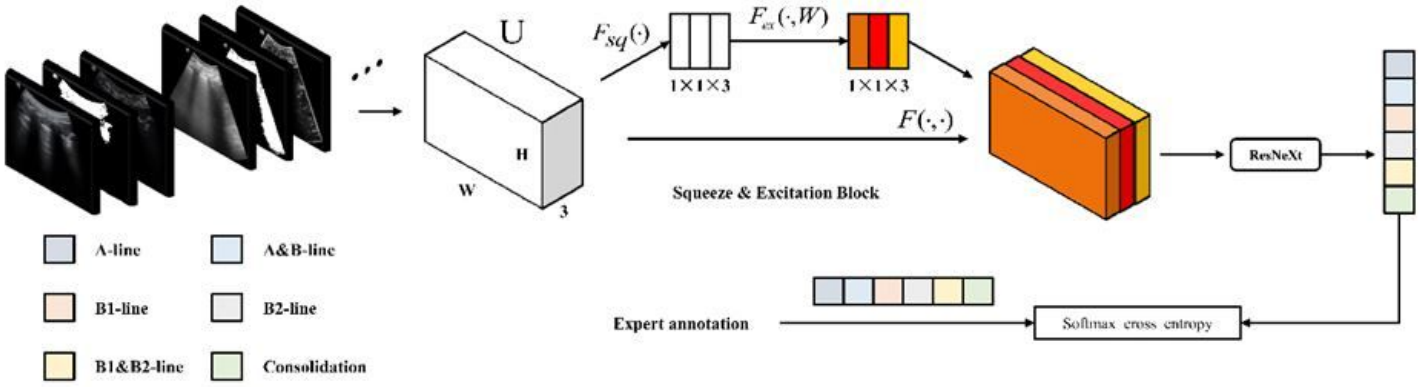

Figure 7

Overview of the proposed SE_ResNeXt for lung congestion degree classification.

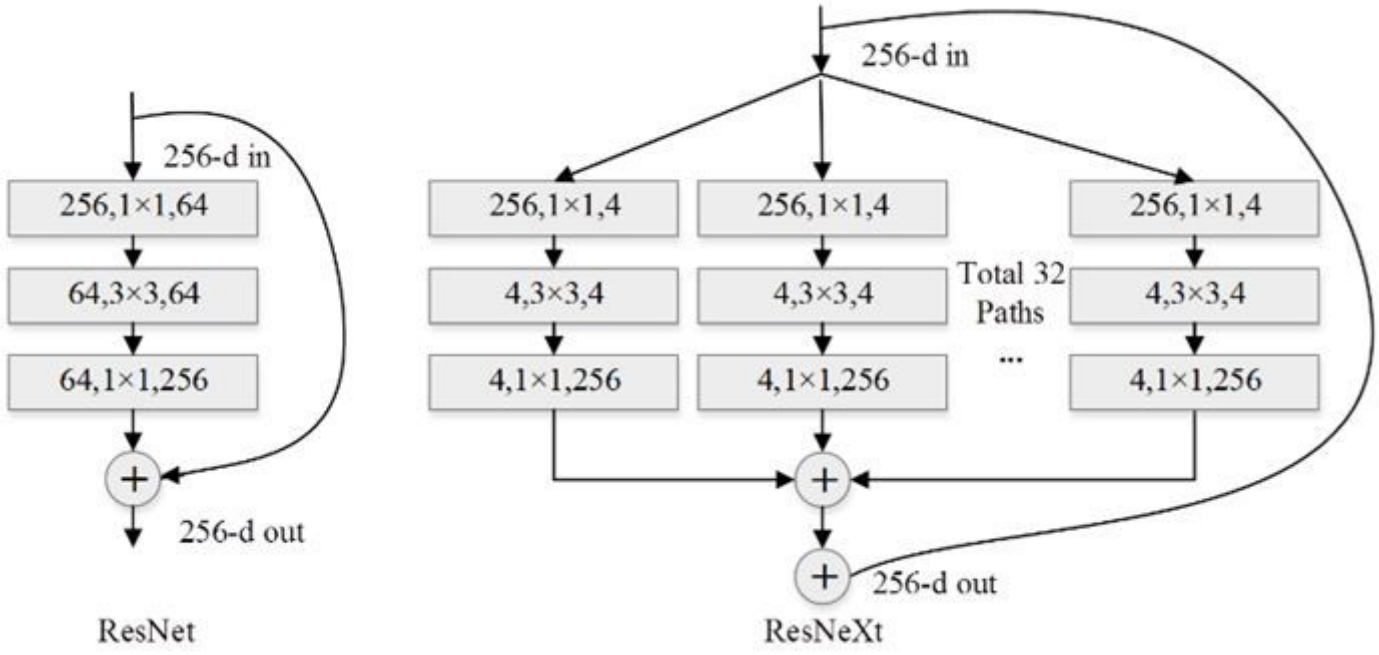

Figure 8

A building block in ResNet and ResNeXt.